Number of particles in fission fragments

Marc Verriere, Nicolas Schunck, and Toshihiko Kawano

Number of Particles in Fission Fragments

Marc Verriere,[1, *] Nicolas Schunck,[2, †] and Toshihiko Kawano[1]

[1] *Los Alamos National Laboratory, Los Alamos, NM 87545, USA*

[2] *Nuclear and Chemical Sciences Division, Lawrence Livermore National Laboratory, Livermore, CA 94551, USA*

(Dated: July 28, 2019)

Background: In current simulations of fission, the number of protons and neutrons in a given fission fragment is almost always obtained by integrating the total density of particles in the sector of space that contains the fragment. The semi-classical nature of this procedure and the antisymmetry of the many-body wave function of the whole nucleus systematically leads to non-integer numbers of particles in the fragment.

Purpose: We seek to estimate rigorously the probability of finding Z protons and N neutrons in a fission fragment, i.e., the dispersion in particle number (both charge and mass). Knowing the dispersion for any possible fragmentation of the fissioning nucleus will improve the accuracy of predictions of fission fragment distributions and the simulation of the fission spectrum with reaction models.

Methods: Given a partition of the full space $\mathbb{R}^3$ in two sectors corresponding to the two prefragments, we discuss two different methods. The first one is based on standard projection techniques extended to arbitrary partitions of space. We also introduce a novel sampling method that depends only on a relevant single-particle basis for the whole nucleus and the occupation probability of each basis function in each of the two sectors. We estimate the number of particles A in the left (right) fragment by statistical sampling of the joint probability of having A single-particle states in the left (right) sector of space.

Results: We use both methods to estimate the charge and mass number dispersion of several scission configurations in ^{240}Pu using either a macroscopic-microscopic approach or full Hartree-Fock-Bogoliubov calculations. We show that restoring particle number symmetry naturally produces odd-even effects in the charge probability, which could explain the well-known odd-even staggering effects of charge distributions.

Conclusions: We discuss two methods to estimate particle number dispersion in fission fragments. In the limit of well-separated fragments, the two methods give identical results. It can then be advantageous to use the sampling method, since it provides a N-body basis for each prefragment, which can be used to estimate fragment properties at scission. When the two fragments are still substantially entangled, the sampling method breaks down and one has to use projector techniques, which gives the exact particle number dispersion even in that limit. Note that in this work, we have assumed that scission configurations could be described well by a static Bogoliubov vacuum: the strong odd-even staggering in the charge distributions could be somewhat attenuated when going beyond this hypothesis.

I. INTRODUCTION

The theoretical understanding of nuclear fission, discovered in 1938 by O. Hahn and F. Strassmann, remains a vexing challenge even to this day. The fission of a heavy atomic nucleus presents a number of conceptual as well as practical difficulties. A fissioning nucleus is a particular example of a quantum many-body system of strongly-interacting Fermions, whose interaction is only known approximately. Fission dynamics is explicitly time-dependent and involves open channels (mostly neutrons, but also photons). From a fundamental perspective, the physics of scission, or how an interacting, quantum many-body system splits into two well-separated, interacting, quantum many-body systems, is very poorly known. Although there has been a considerable body of experimental work on fission in general, the most accurate data involves the decay of the fission fragments. The mechanism by which these fragments are formed in the first place must be described by theory.

Several approaches have been developed over the years to describe the fission process. Since fission times are rather slow compared with single-particle types of excitations [1, 2], quasi-static approaches are well justified. Most incarnations of these approaches rely on identifying a few collective variables that drive the fission process, mapping out the potential energy surface in this collective space (which fixes all properties of fission fragments) and computing the probability for the nucleus to be at any point on the surface, e.g. with semi-classical dynamics such as Langevin [3–5], random walk [6–9] or with fully quantum-mechanical dynamics such as the time-dependent generator coordinate method [10–13]. One major limitation of these approaches is the need to identify scission configurations in the potential energy surface, that is, the arbitrary frontier that separates configurations where the nucleus is whole from those where it has split into two fragments [14–16]. In practice, such scission configurations happen to always be characterized by non-integer values of average particle numbers in the fragments.

The arbitrariness of the very concept of scission is strongly mitigated in explicitly non-adiabatic theories of fission such as the various formulations of time-dependent nuclear density functional theory [1, 2, 17–23]. Since

these approaches simulate the real-time evolution of the nucleus and explicitly conserve energy, one can obtain excellent estimates of fission fragment properties well past the actual scission point [1, 2, 18]. However, these theories still simulate the evolution of the fissioning nucleus instead of the fragments themselves: the latter remain entangled even after scission and thus have also non-integer values of proton and neutrons [20]. Particle number symmetry in the fragments could in principle be restored by using standard projection techniques. This approach was pioneered initially in the case of particle transfer in heavy ion fusion reactions [24–27]. However, as we will discuss below, projection techniques do not allow to identify independent configurations in the fragments. While this does not impact the estimate of primary charge or mass yields, it would be very useful to have access to a basis of N-body Slater determinants of particles to calculate other observables.

Our goal is thus to explore an alternative method to estimate the number of particles in the fission fragments. More precisely, given a description of the fissioning system by a A-body Slater determinant or a quasiparticle vacuum, we seek to determine both the probability that the total N-body wave function contains a Slater determinant of particle with A_1 (A_2) particles in the left (right) fragment, both A_1 and A_2 being integers and $A_1 + A_2 = A$, as well as a suitable basis of single-particle states to describe them. In this paper, we propose a new method that only depends on a physically-relevant single-particle basis for the fissioning nucleus and a set of occupation probabilities.

We present our theoretical framework in Section II. This includes some general notations, the presentation of our Monte-Carlo sampling method, and a reminder of projection techniques adapted to the case of fission fragments. Section III is focused on the validation and numerical implementation of the sampling method. In Section IV, we study in more details the fragmentation probabilities for scission configurations in ^{240}Pu, before concluding in Section V.

II. THEORETICAL FORMALISM

The prediction of the primary mass/charge distribution in fission can be decomposed in three steps [16]. First, one calculates the energy of the fissioning system for a set of configurations with different geometric shapes or constraints. This potential energy surface (PES) is divided into two regions, one where the nucleus has split into two fragments, the other where it has not; scission configurations correspond to the frontier between the two regions. In a second step, one estimates the probability to populate each scission configuration. This can be done either semi-classically by solving the Langevin equation as in [5, 28–36] or with a random walk approach [6–9, 37], or more microscopically by using time-dependent configuration techniques such as the time-dependent generator coordinate method with the Gaussian overlap approximation (TDGCM-GOA) [11, 12, 38–42]. Finally the result of the time-dependent evolution are coupled with an estimate of fragment properties to estimate the actual distribution of nuclear observables such as charge, mass, total kinetic energy (TKE), etc.

In the case of charge and mass distributions, the last step of the procedure outlined above involves estimating the particle number in the fission fragments. Until recently, all fission calculations have used a semi-classical estimate of the average particle number based on integrating the one-body density. Below, we describe two methods to obtain integer values of particle number. The first method, which is developed in this paper, involves a Monte-Carlo sampling of single-particle configurations. Its main advantage is that it indirectly provides a set of single-particle wave functions for each of the fragments, which could then be used to estimate quantities such as, e.g., the level density. The second method is based on extending standard projection techniques to arbitrary space partitionings and was introduced originally by Simenel in [24] for Slater determinants and later extended in [25] to the case of superfluid systems.

A. Space partitioning

Let us first assume that the state $|\Phi\rangle$ of the fissioning system is a Slater determinant of particles,

$$|\Phi\rangle \equiv \prod_{k=0}^{A-1} \hat{c}_k^\dagger |0\rangle, \tag{1}$$

where $|0\rangle$ is the particle vacuum. The operator $\hat{c}_k^\dagger$ creates a fermion in the single-particle state k and reads

$$\hat{c}_k^\dagger = \int_{\mathcal{V}} \mathrm{d}^3\boldsymbol{r}\, \varphi_k(\boldsymbol{r})\hat{c}^\dagger(\boldsymbol{r}), \tag{2}$$

where $\varphi_k(\boldsymbol{r})$ is the single-particle wave function for state k and the operator $\hat{c}^\dagger(\boldsymbol{r})$ creates a well-localized fermion at point $\boldsymbol{r}$ (we omit spin and isospin degrees of freedom for the sake of simplicity). Recall that the set of all functions $\varphi_k(\boldsymbol{r})$ form a basis of the $\mathcal{L}_2$ Hilbert space of square-integrable functions.

We also assume that it is possible to partition the full space $\mathcal{V} \equiv \mathbb{R}^3$ into two sectors $\mathcal{V}_0$ and $\mathcal{V}_1$ such as $\mathcal{V}_0$ ($\mathcal{V}_1$) is the region where the left (right) fragment is localized. Such a partitioning could, for instance, be defined by introducing the coordinates of a neck between the two prefragments at scission, as illustrated schematically in Figure 1. The two prefragments are separated by the red line located at the neck position. It is then always possible to decompose the single-particle wave functions into

$$\varphi_k(\boldsymbol{r}) = \alpha_k^{(0)}\varphi_k^{(0)}(\boldsymbol{r}) + \alpha_k^{(1)}\varphi_k^{(1)}(\boldsymbol{r}), \tag{3}$$
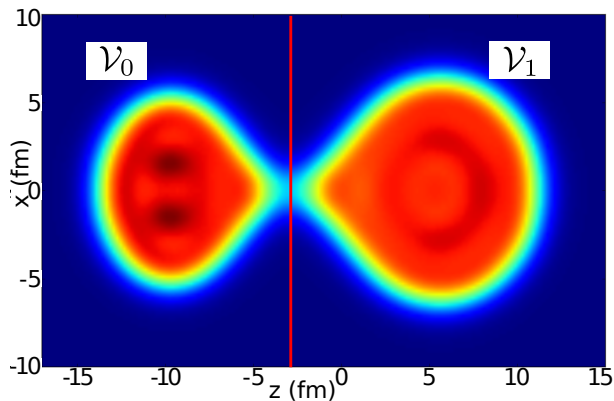
FIG. 1. Illustration of the partition of the space $\mathcal{V}$ into $\mathcal{V}_0$ and $\mathcal{V}_1$ using the local density. The color scale corresponds to the value of the local density associated with a Slater determinant $|\Phi\rangle$. The red line separates $\mathcal{V}_0$ (to the left of the line) and $\mathcal{V}_1$ (to the right of the line).

where $\varphi_k^{(p)}(\boldsymbol{r})$ is defined in $\mathcal{V}_p$ ($p = 0, 1$) and $\alpha_k^{(p)}$ are normalization coefficients obtained by integrating the single-particle wave functions in the domain $\mathcal{V}_p$,

$$\alpha_k^{(p)} = \sqrt{\int_{\mathcal{V}_p} d^3\boldsymbol{r}\, |\varphi_k(\boldsymbol{r})|^2}. \tag{4}$$

In terms of operators, the expansion of Eq.(3) simply translates into

$$\hat{c}_k^\dagger = \alpha_k^{(0)} \hat{c}_k^{(0)\dagger} + \alpha_k^{(1)} \hat{c}_k^{(1)\dagger}. \tag{5}$$

The ladder operators $\hat{c}_k^{(0)\dagger}$, $\hat{c}_k^{(1)\dagger}$ and their Hermitian conjugates verify the following anti-commutation relations ($p, r = 0, 1$)

$$\left\{ \hat{c}_k^{(p)\dagger}, \hat{c}_l^{(r)\dagger} \right\} = \left\{ \hat{c}_k^{(p)}, \hat{c}_l^{(r)} \right\} = 0 \tag{6}$$

$$\left\{ \hat{c}_k^{(p)\dagger}, \hat{c}_l^{(r)} \right\} = \delta_{pr} \int d\boldsymbol{r}\, \varphi_k^{(p)}(\boldsymbol{r}) \varphi_l^{(r)*}(\boldsymbol{r}) \tag{7}$$

In the general case, $\left\{ \hat{c}_k^{(p)\dagger}, \hat{c}_l^{(p)} \right\} \neq 0$ when $k \neq l$. However, it is always possible to restore all the Fermion anti-commutation relations by orthonormalizing (for example with the Gram-Schmidt procedure) the bases $\{\hat{c}_k^{(0)\dagger}\}$ and $\{\hat{c}_k^{(1)\dagger}\}$ separately. Given these prerequisites, the goal of our method is to estimate the relative probability of finding a many-body state with N_p particles in the subspace $\mathcal{V}_p$.

B. Monte-Carlo Approach

We first present a method that only requires the coefficients (4). Calculating them requires in turn only two ingredients: a set of single-particle wave functions and a partitioning of $\mathbb{R}^3$. Let us emphasize that from a mathematical/algorithmic point of view, the partitioning of the space is entirely arbitrary. We refer to our method as Monte Carlo (MC) sampling.

1. Orthonormal Bases

We first introduce the general principles of our method for the idealized case where the $\varphi_k^{(p)}$ form an orthonormal basis of $\mathcal{V}_p$. We emphasize very clearly that in the most general case, this condition is *not* satisfied. In the context of fission, however, it can be approached asymptotically in the limit of infinitely-separated fragments. In practice, it is reasonable to assume that scission configurations will sufficiently well approximate this limiting case so that the method can still provide reasonable estimates of the particle numbers.

If the $\varphi_k^{(p)}$ form an orthonormal basis of $\mathcal{V}_p$, then the Fermion anti-commutation relations between the corresponding s.p. operators are satisfied. Let us insert Eq. (5) in Eq. (1). We obtain

$$|\Phi\rangle = \sum_{\substack{\boldsymbol{p}=(p_0,\dots,p_{A-1}) \\ p_k \in (0,1)}} \left[\prod_{k=0}^{A-1} \alpha_k^{(p_k)} \right] \left[\prod_{k=0}^{A-1} \hat{c}_k^{(p_k)\dagger} \right] |0\rangle. \tag{8}$$

In Eq. (8), we sum over all possible A-uplets of 0 and 1. Since we assume that the $\hat{c}_k^{(0)\dagger}$ and $\hat{c}_k^{(1)\dagger}$ correspond to orthonormal bases, the A-body state $|\boldsymbol{p}\rangle$ defined by

$$|\boldsymbol{p}\rangle = \prod_{k=0}^{A-1} \hat{c}_k^{(p_k)\dagger} |0\rangle \tag{9}$$

is a Slater determinant. By using the Fermion anti-commutation relations of the $\hat{c}_k^{(p)\dagger}$, we see that the set of all the possible $|\boldsymbol{p}\rangle$ forms an orthonormal basis of the A-body space. By construction, each state $|\boldsymbol{p}\rangle$ is an eigenvector of the particle number operators for *both* $\mathcal{V}_0$ and $\mathcal{V}_1$ and contains two sets of particles. The first set is completely in $\mathcal{V}_0$ and will contribute only to the left fragment, the second set is completely in $\mathcal{V}_1$ and will contribute only to the right fragment. Therefore, we can easily calculate the number of particles in the left (right) fragment for $|\boldsymbol{p}\rangle$, $N_0(\boldsymbol{p})$ ($N_1(\boldsymbol{p})$). Since p_k is either 0 or 1, it is easy to show that

$$N_0(\boldsymbol{p}) = \sum_{k=0}^{A-1} (1 - p_k), \qquad N_1(\boldsymbol{p}) = \sum_{k=0}^{A-1} p_k. \tag{10}$$

and that $N_0(\boldsymbol{p}) + N_1(\boldsymbol{p}) = A$ as expected. We can therefore rewrite Eq. (8) in the form

$$|\Phi\rangle = \sum_{N_0=0}^{A-1} c_{N_0} |N_0\rangle, \tag{11}$$

where $|N_0\rangle$ is the normalized component of $|\Phi\rangle$ with N_0

Fermions in the left fragment, which is given by

$$|N_0\rangle \equiv \frac{1}{c_{N_0}} \sum_{\substack{\boldsymbol{p}=(p_0,\ldots,p_{A-1}) \\ N_0(p)=N_0}} \left[\prod_{k=0}^{A-1} \alpha_k^{(p_k)}\right] |p\rangle, \qquad (12)$$

$$c_{N_0} \equiv \sqrt{\sum_{\substack{\boldsymbol{p}=(p_0,\ldots,p_{A-1}) \\ N_0(p)=N_0}} \left(\prod_{k=0}^{A-1} \alpha_k^{(p_k)}\right)^2}. \qquad (13)$$

Let us consider two different states $|N_0\rangle$ and $|N_0'\rangle$ such that $N_0 \neq N_0'$. The states $|N_0\rangle$ and $|N_0'\rangle$ are expanded on disjointed subsets of the basis $|\boldsymbol{p}\rangle$. Since we already showed that this basis is orthonormal, it implies that the states $|N_0\rangle$ and $|N_0'\rangle$ are orthogonal and the squared norm of $|N_0\rangle$ is given by

$$\langle N_0|N_0\rangle = 1. \qquad (14)$$

We can now define the probability $\mathbb{P}_0(N_0)$ to measure the left fragment with N_0 particles as

$$\mathbb{P}_0(N_0) \equiv \langle\Phi|N_0\rangle\langle N_0|\Phi\rangle = c_{N_0}^2. \qquad (15)$$

Calculating all the probabilities $\mathbb{P}_0(N_0)$ using (13) and (15) scales like $A \times 2^A$. While this can certainly be done for nuclei with $A < 30$, it becomes problematic in heavy systems such as actinides. Instead, we can use a statistical approach to sample this probability. Specifically, we will use Monte-Carlo sampling techniques to estimate the distribution of probability. For a A-body Slater determinant, this only requires drawing A uniformly-distributed random numbers at each iteration.

2. Non-orthonormal Bases

As briefly mentioned earlier, the set of single-particle functions $\varphi_k^{(p)}(\boldsymbol{r})$ does not, in general, form a basis of the subspace $\mathcal{V}_p$. Note that $\mathcal{V}_p$ is a Hilbert space very similar to the usual Hilbert space of square-integrable functions $\mathcal{L}^2(\mathbb{R}^3)$. Therefore, it could in principle be equipped with a proper basis. The problem is that such bases are not necessarily related to the original basis of functions $\varphi_k(\boldsymbol{r})$ through a simple relation such as Eq.(3).

The only case where the functions entering Eq.(3) do form a basis of their respective Hilbert space is when the two fragments are infinitely separated. This can be most easily seen from exactly solvable models. In one dimension, for example, a double harmonic oscillator potential of the type $V(x) = \frac{\omega^2}{8a^2}(x-a)^2(x+a)^2$, somewhat simulates the potential well between two (identical) pre-fragments separated by an average distance of $2a$. At the limit of infinite separation ($a \to \infty$), the two harmonic oscillators completely decouple and the solution of the Schrödinger equation for the full system tends toward the sum of two Harmonic oscillators shifted by $\pm a$; see, e.g., [43] for a comprehensive presentation. Note that a

full treatment of the problem with path integrals would still lead to a non-zero tunneling probability between the two systems, which is beyond the scope of this work.

The point of this short discussion is that our hypothesis that the two sets of functions $\varphi_k^{(0)}$ and $\varphi_k^{(1)}$ are *approximately* orthonormal should be reasonable.

3. Inclusion of Pairing Correlations

Pairing correlations play an essential role in the fission process [1, 18, 21]. In static calculations, they are typically described within the BCS or HFB approximations (with or without projection). In both cases, one can always define a set of single-particle wave functions $\varphi_k(\boldsymbol{r})$ associated with the operators $\hat{c}_k^\dagger$. This basis can be, for instance, made of the eigenstates of some realistic average potential (macroscopic-microscopic approaches) or of the nuclear mean field (Hartree-Fock theory), or it can be the canonical basis in the HFB theory. Together with single-particle states, pairing theories also provide the occupation amplitudes u_k and v_k, such that $u_k^2 + v_k^2 = 1$.

Based on these remarks, one can extend our method of calculation for the probability $\mathbb{P}(N_0)$ of finding N_0 particles in the left fragment in presence of pairing correlations by performing two consecutive statistical samplings. We first draw random sets of A occupied levels from the canonical basis based on the values of the probability amplitudes u_k^2 and v_k^2. For any such sample, we can then apply the method outlined in the previous sections. In more details, the procedure is thus the following:

1. For each energy level k in the canonical basis, draw a uniformly-distributed random number $0 \leq r_k \leq 1$ and select the level for occupation if $r_k \leq v_k^2$. The Slater determinant $|\tilde{\Phi}_{\boldsymbol{p}}\rangle$ thus formed out of all the occupied levels occurs with the probability $\mathbb{P}(\boldsymbol{p})$

$$\mathbb{P}(\boldsymbol{p}) = \prod_{\substack{o \\ p_o=1}} v_o^2 \prod_{\substack{n \\ p_n=0}} u_n^2; \qquad (16)$$

2. For each such state $|\tilde{\Phi}_{\boldsymbol{p}}\rangle$ with good particle number, we calculate the probability $\mathbb{P}(N_0)$ that the left fragment has N_0 particles by using the method presented earlier;

3. We repeat this two-step sampling as many times as needed for the final probability distributions $\mathbb{P}(N_0)$ to converge. In practice, this requires of the order of a few thousands of iterations.

It is important to realize that the first step of the procedure described above can be used to estimate the probability $\mathbb{P}(N_0)$ that an arbitrary BCS or HFB state contains exactly N_0 particles. Therefore, it is an alternative way to project on particle number without introducing any projector. We will take advantage of this observation to validate our method.

C.   Projectors Method

The number of particles in fission fragments can also be recovered by using projector techniques as developed in [24, 25]. Here, we give a brief summary of projection with emphasis on practical aspects and possible differences between the MC sampling presented previously.

In the standard approach to projection, see e.g. [44, 45], the particle-number projection operator $\hat{P}^q(N)$ reads

$$\hat{P}^q(N) \equiv \frac{1}{2\pi} \int_0^{2\pi} \mathrm{d}\theta \, e^{i\theta(\hat{N}^q - N)}, \tag{17}$$

where $q = $ neutron,proton is the type of particle and $\hat{N}^q$ is the particle number operator. The idea in [24] is the following: instead of using the particle number on the full space, one may define an operator $\hat{N}_p^q$ that count the number of particles only in the partition $\mathcal{V}_p$. This operator can be written

$$\hat{N}_p^q \equiv \int dx \, \hat{c}^\dagger(x)\hat{c}(x)\Theta_p(\boldsymbol{r}), \tag{18}$$

where, as usual, we note $x \equiv (\boldsymbol{r}, \sigma, q)$ and $\int dx \equiv \sum_\sigma \int d^3\boldsymbol{r}$. In (18), p indexes the partitions $\mathcal{V}_p$ and $\Theta_p(\boldsymbol{r})$ represents the indicator function of $\mathcal{V}_p$, i.e.

$$\Theta_p(\boldsymbol{r}) \equiv \begin{cases} 1 & \text{if } \boldsymbol{r} \in \mathcal{V}_p, \\ 0 & \text{otherwise.} \end{cases} \tag{19}$$

Obviously, we have the operatorial equality

$$\sum_p \hat{N}_p^q = \hat{N}^q. \tag{20}$$

In Ref. [24], $\mathcal{V}_p$ is denoted R and corresponds to the set of points with a positive value of x. In this case, $\Theta_R(\boldsymbol{r}) \equiv \Theta(x)$ and therefore, we obtain the equation (1) of [24]. Based on this definition, we can construct $\hat{P}_p^q(N)$, the particle number projector on the partition $\mathcal{V}_p$, as follows

$$\hat{P}_p^q(N) \equiv \frac{1}{2\pi} \int_0^{2\pi} \mathrm{d}\theta \, e^{i\theta(\hat{N}_p^q - N)}. \tag{21}$$

Computing the action of $\hat{P}_p^q(N)$ on an arbitrary HFB vacuum $|\Phi\rangle$ can be done by defining shift operators $\hat{z}_p \equiv z^{\hat{N}_p^q}$ with $z = e^{i\theta}$ and following the same approach as in [46]. By working directly with these field operators in coordinate space, one may show that

$$\left(\hat{N}_p^q\right)^n \hat{c}^\dagger(x) = \hat{c}^\dagger(x)\left[\Theta_p(x) + \hat{N}_p^q\right]^n, \tag{22}$$

which leads to

$$\hat{z}_p \hat{c}^\dagger(x) \hat{z}_p^{-1} = e^{i\theta\Theta_p(x)} \hat{c}^\dagger(x). \tag{23}$$

By introducing the expansion of the field operators $\hat{c}^\dagger(x)$ on a basis, we arrive at

$$b_k^\dagger(\theta) \equiv \hat{z}_p \hat{c}_k^\dagger \hat{z}_p^{-1} = \sum_l F_{kl}(\theta)\hat{c}_l^\dagger, \tag{24}$$

with

$$F_{kl}(\theta) = \int dx \, \varphi_k^*(x)\varphi_l(x)e^{i\theta\Theta_p(x)} = \delta_{kl} + S_{kl}^{(p)}(e^{i\theta} - 1), \tag{25}$$

where $S_{kl}^{(p)}$ is the overlap matrix of the basis $\varphi_k^{(p)}$. We then find that the action of the shift operator on the HFB vacuum reads, in the canonical basis,

$$\hat{z}_p|\Phi\rangle = \prod_{k>0}\left[u_k + v_k b_k^\dagger(\theta)b_{\bar{k}}^\dagger(\theta)\right]|0\rangle. \tag{26}$$

The calculation of the norm overlap can then be efficiently computed with the Pfaffian techniques of [47] as outlined in [20].

In order to estimate the probability $\mathbb{P}_p^q(N)$ to find N nucleons of type q in the spatial partition $\mathcal{V}_p$, we must also make sure that the total number of particles in the fissioning system is restored. Therefore, the probability $\mathbb{P}_p^q(N)$ involves a double projection

$$\mathbb{P}_p^q(N) \equiv \frac{\langle\Phi|\hat{P}_p^q(N)\hat{P}^q(N_{\text{tot}})|\Phi\rangle}{\langle\Phi|\hat{P}^q(N_{\text{tot}})|\Phi\rangle}, \tag{27}$$

where N_{tot} is the total number of particles of species q for the fissioning nucleus. As mentioned in [25], the double projection involves the integration over two gauge angles θ and θ'. One can easily show that the rotated wave function will simply read

$$\hat{z}_p\hat{z}|\Phi\rangle = \prod_{k>0}\left[u_k + v_k b_k^\dagger(\theta, \theta')b_{\bar{k}}^\dagger(\theta, \theta')\right]|0\rangle, \tag{28}$$

where $b_k^\dagger(\theta, \theta')$ is given by (24), only replacing $F_{kl}(\theta)$ by $F_{kl}(\theta, \theta') = F_{kl}(\theta)e^{i\theta'}$.

III.   PROOFS OF PRINCIPLE

In this section, we study how the MC sampling method can be used to restore particle number. First, we validate the approach against the projector method in a "standard" case of particle number restoration for a fully-paired HFB vacuum. We then apply MC sampling to estimate fragmentation probabilities in different subspaces and analyze the numerical convergence of the method.

A.   Validation

The validation consists in using our sampling method to compute the coefficients c_N of the expansion of an arbitrary HFB state $|\Phi\rangle$ on good-particle number Slater determinants,

$$|\Phi\rangle = \sum_N c_N|N\rangle, \quad |N\rangle = \frac{\hat{P}(N)|\Phi\rangle}{\sqrt{\langle\Phi|\hat{P}(N)|\Phi\rangle}}. \tag{29}$$

This is done simply by following Step 1 of the procedure discussed in Section II B 3. We chose (arbitrarily) the nucleus $Z = 60$ and $N = 70$ for the tests. We used the code HFBTHO 3 [48] to solve the HFB equation for this nucleus in a deformed HO basis of 16 shells (oscillator length: $b_0 = 2.0$ fm, $\beta_2 = 0.2$). We took the SkM* parametrization of the Skyrme functional, a surface-volume pairing interaction with $V_{0n} = V_{0p} = -250$ MeV and an infinite quasiparticle cutoff. Note that it does not matter if these characteristics are realistic or not: they were chosen exclusively to make sure there was a substantial amount of pairing correlations for both protons and neutrons.

TABLE I. Comparison of the sampling method and exact particle number projection for the calculation of the coefficients of the expansion of Eq. (29) for both protons and neutrons; see text for additional details.

Number	$|c_N|^2$		$|c_Z|^2$	
	PNP	sampling	PNP	sampling
N	0.3706	0.3707	0.3906	0.3905
N-2	0.3208	0.3207	0.3363	0.3362
N-4	0.2079	0.2079	0.1971	0.1972
N-6	0.1006	0.1007	0.0760	0.0760

We then projected the HFB solution on $N_0 = 70$, 68, 66 and 64 as well as on $Z_0 = 60$, 58, 56 and 54 using the Fomenko discretization of the particle number projector with $L = 13$ gauge points. Since number parity is conserved in this case, the coefficients c_N of the expansion of Eq. (29) are then simply given by [49–51]

$$c_N^2 = \langle \Phi | \hat{P}(N) | \Phi \rangle = \frac{1}{L} \sum_{l=0}^{L-1} \langle \Phi | e^{i\theta_l (\hat{N} - N)} | \Phi \rangle, \qquad (30)$$

where $\theta_l = \pi l / L$ are the gauge angles. To ensure that $\sum_{N \in I} |c_N|^2 = 1$ for our subset I of particle numbers, we renormalized the coefficients. The table I compares the results obtained with direct projection and with our sampling method applied on the canonical basis. They are exact to within 10^{-4}, which corresponds to the precision of the sampling.

B. Fragmentation Probabilities

We now examine how MC sampling can be used to estimate the particle number in different subspaces. For simplicity, we focused on the nucleus ^{240}Pu. For this proof of principle, we consider a macroscopic-microscopic approach where the shape of the nucleus is described by the Matched Quadratic Surface (3QS) parametrization [52–54]. The single-particle states are obtained by solving the Schrödinger equation for a few specific elongated shapes listed in Table II in an axial harmonic oscillator (HO) basis of $N_{sh} = 35$ shells. Pairing correlations are treated in

the Lipkin-Nogami approximation with a seniority pairing force characterized by Eq. (107) of [55]. We used an energy window of ± 5 MeV around the Fermi level to define our valence space; further details of the theoretical framework can be found in [55].

The quantities A_L and Z_L listed in Table II refer to the mass and charge of the prefragments obtained by integrating the one-body local density at the left and right of the neck position. The latter is defined as the point with the lowest density between the two prefragments.

TABLE II. Characteristics of scission configurations: shape parameters and average mass and charge fragmentation.

Shape	α_2	α_3	σ_1	σ_2	σ_3	A_L	Z_L
I	0.30	0.192	3.500	-0.576	0.640	99.61	39.78
II	0.25	0.203	3.889	-0.365	0.810	101.33	40.91
III	0.25	0.250	3.500	-0.450	1.000	102.36	41.82
IV	0.20	0.605	3.182	-0.545	1.210	112.29	44.95

We have calculated the fragmentation probabilities associated with the configurations of Table II. We drew $n_{pair} = 10000$ A-body Slater determinants and for each of them used $n_{loc} = 10000$ Monte-Carlo samples to estimate the number of particles in the fragments. Since the configurations are not fully scissioned, we take into account the uncertainty associated with the position z_{neck} of the neck by assuming that z_{neck} follows a normal distribution $\mathcal{N}(\bar{z}_{neck}, A_{neck} \times Q_{neck})$, where $\bar{z}_{neck}$ is the position of the minimum between the two fragments of the local density along the z-axis, $A_{neck} = 1$ fm/nuc and Q_{neck} is the average value of the Gaussian neck operator [15, 56].
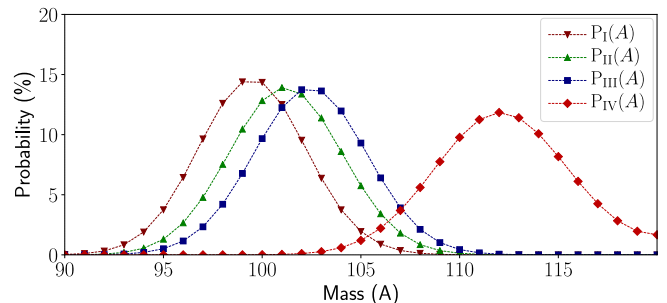
FIG. 2. Mass fragmentation probabilities (light fragment) for all the configurations listed in Table II.

The mass fragmentation probabilities are shown in Figure 2. We note that all curves are smooth and are peaked near the values of A corresponding to the geometric split between the fragments. There is no visible odd-even staggering for any of the mass probabilities. In the case of the charge fragmentation probabilities shown in Figure 3, we note that the maximum of each curve is always associated with an even number of protons. Moreover, the probability for any even proton number is always higher than the probability of any of the two odd-proton neighbors. In other words, we observe a clear odd-even staggering

(OES). The different behavior of the mass and charge fragmentations is most likely caused by the Coulomb potential between the fragments, which increases the height of the effective barrier between them and therefore tends to localize the protons better than the neutrons.
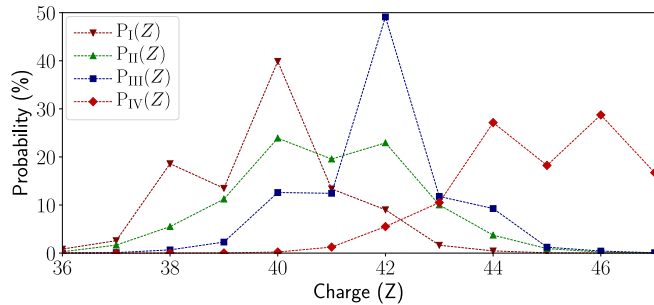

FIG. 3. Charge fragmentation probabilities (light fragment) for all the configurations listed in Table II

Note that the fragmentation probabilities shown in Figures 2-3 cannot be compared to experimental data [57, 58]: they give only the dispersion around 4 specific fragmentations. In contrast, experimental fission fragment distributions include all possible fragmentations of the compound nucleus. To compare with experimental data, the first step is to explicitly simulate the nuclear dynamics, e.g., with semi-classical methods such as Langevin or random walk [5–9, 28–37] or microscopic methods such as the time-dependent generator coordinate method [11, 12, 38–42]. This would provide the probability distribution $\mathbb{P}(\mathcal{S})$ for the nucleus to be in a given scissionned or quasi-scissionned state $\mathcal{S}$. The second step would be to fold the probability distribution thus obtained with the probabilities $\mathbb{P}_{\mathcal{S}}(A)$ or $\mathbb{P}_{\mathcal{S}}(Z)$ that our method provides via

$$Y(X) = \sum_{\mathcal{S}} \mathbb{P}(\mathcal{S})\mathbb{P}_{\mathcal{S}}(X), \quad X = Z, A \quad (31)$$

$$Y(A,Z) = \sum_{\mathcal{S}} \mathbb{P}(\mathcal{S})\mathbb{P}_{\mathcal{S}}(A)\mathbb{P}_{\mathcal{S}}(Z). \quad (32)$$

Note that even if we do not consider correlations between protons and neutrons in the fragment probabilities in our method, the yields $Y(A,Z)$ obtained with the dynamics contains them.

C. Numerical Convergence

The MC method of Sec. II B is statistical and relies on sampling a probability distribution. When pairing correlations are included, the sampling is characterized by two numbers: n_{pair}, the number of draws of the particle Slater determinants (first step of the algorithm presented in II B 3, page 4), and n_{loc}, the number of draws of a localized Slater determinant of A particles from the left/right basis (c.f. Eq. (8)). Here, we evaluate the uncertainty

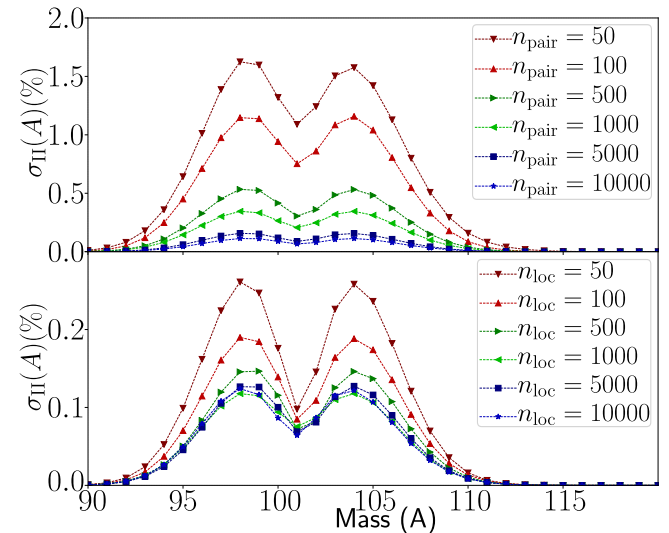associated with these two integers for the particular case of configuration II in Table II.

FIG. 4. Standard deviations associated with the probabilities to measure the light fragment with a mass A for the shape II. Top: For different values of n_{pair} and with $n_{\text{loc}} = 10000$. Bottom: For different values of n_{loc} and with $n_{\text{pair}} = 10000$
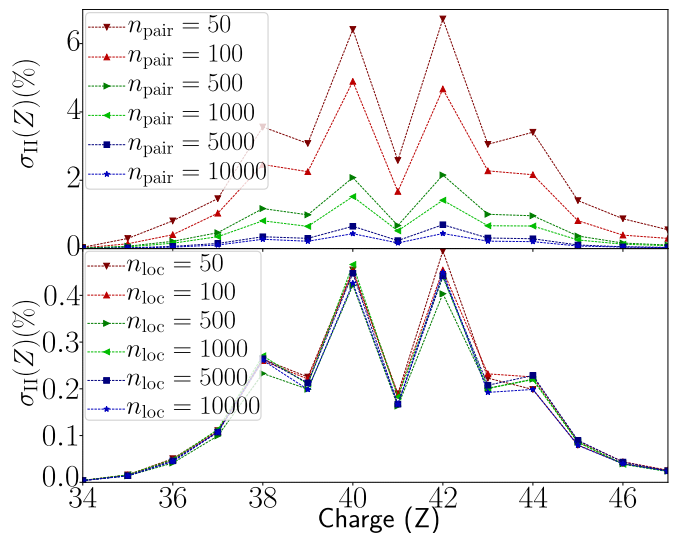

FIG. 5. Same as Figure 4 for the charge fragmentations.

We considered 12 cases: $n_{\text{pair}} = 50, 100, 500, 1000, 5000, 10000$ with $n_{\text{loc}} = 10000$; and $n_{\text{pair}} = 10000$ with $n_{\text{loc}} = 50, 100, 500, 1000, 5000, 10000$. For each of them, we calculated the fragmentation probability in mass and charge $S = 200$ times. We then calculated the unbiased estimator of the standard deviation $\sigma_{\text{II}}(X)$ for the distributions in mass and in charge using the following expression, for $X = A, Z$,

$$\sigma_{\text{II}}(X) \equiv \sqrt{\frac{1}{S-1} \sum_{k=0}^{S-1} \left[Y_{\text{II}}^{(k)}(X) - \bar{Y}_{\text{II}}(X)\right]^2}, \quad (33)$$

where $Y_{\mathrm{II}}^{(k)}(X)$ is the k-th calculation of the yields with our method and $\bar{Y}_{\mathrm{II}}(X)$ is the mean value of all the $Y_{\mathrm{II}}^{(k)}(X)$. The standard deviations are shown on Figure 4 for the mass distributions, and on Figure 5 for the charge distributions. The most sensitive parameter is n_{pair} with an improvement of 1.6% of the standard deviations on the masses and 5.5% on the charges between the cases $n_{\mathrm{pair}} = 50, n_{\mathrm{loc}} = 10000$ and $n_{\mathrm{pair}} = n_{\mathrm{loc}} = 10000$ as shown on the upper panels of Figure 4 and Figure 5. For all the cases with $n_{\mathrm{pair}} = 10000$, the standard deviations are always below 0.5% and the improvement of the standard deviations is below 0.2% for the masses and not visible for the charges between the cases $n_{\mathrm{loc}} = 50$ and $n_{\mathrm{loc}} = 10000$.
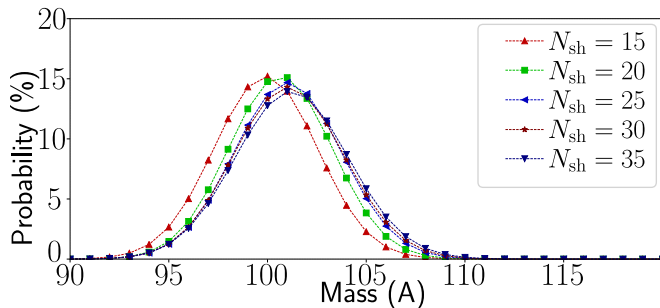
FIG. 6. Probabilities to measure the light fragment with a mass A for the shape II for different number of shells N_{sh} in the basis.
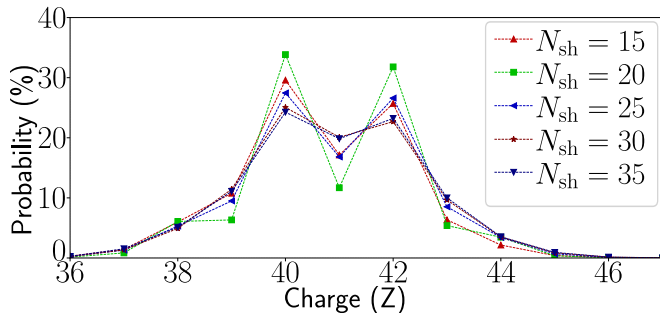

FIG. 7. Same as Figure 6 for the charge of the light fragment.

The two other numerical parameters in our method are the number of shells N_{sh} and the truncation in the BCS occupation numbers v_{thresh}^2. To analyze the impact of N_{sh}, we have calculated the fragmentation probabilities in mass and charge for $N_{\mathrm{sh}} = 15, 20, 25, 30, 35$, in the case of the configuration II. The corresponding curves are presented in Figure 6 and Figure 7. The increase of the number of shells shifts the most probable mass of the light fragment from $A = 100$ to $A = 101$ (and therefore shifts the most probable mass of the heavy fragment from $A = 140$ to $A = 139$). The increase of the number of shells does not change the most probable charge of the fragments. However, it drastically reduces the odd-even staggering in the charge distribution between the cases

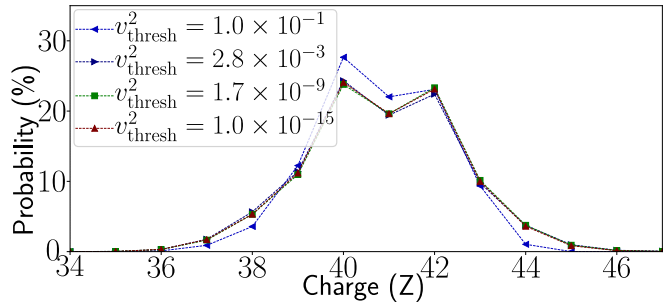$N_{\mathrm{sh}} = 15$ and $N_{\mathrm{sh}} = 35$.

FIG. 8. Probabilities to measure the light fragment with a charge Z for the shape II different values v_{thresh}^2 of the occupation numbers threshold.

To study the influence of the BCS occupations v_{thresh}^2, we have calculated the fragmentation probability in mass and charge for the 4 cases $v_{\mathrm{thresh}}^2 = 1.0 \times 10^{-1}, 2.8 \times 10^{-3}, 1.7 \times 10^{-9}, 1.0 \times 10^{-15}$. The corresponding probabilities are shown in Figure 8 for the charge distributions only. All the distributions, for the mass and the charges, have converged below 1% for $v_{\mathrm{thresh}}^2 \leq 2.8 \times 10^{-3}$.

IV. NUMBER OF PARTICLES AT SCISSION

In this section, we apply both the MC sampling and projector methods to estimate the dispersion in particle number of realistic scission configurations for the case of $^{240}\mathrm{Pu}$.

A. Macroscopic-microscopic Calculations

First, we compare our approach with the projector method presented in [24, 25] for the macroscopic-microscopic approach. The Schödinger equation was solved in a basis of $N_{\mathrm{sh}} = 35$ shells. Pairing correlations are treated in the same way as in Sec. III C. We consider a scission configuration in $^{240}\mathrm{Pu}$ characterized by the following values of the 3QS parameters: $r_{\mathrm{neck}} = 2.50$ fm, $\alpha_2 = 0.448$, $\alpha_3 = 0.6259$, $\sigma_1 = 3.0613$, $\sigma_2 = -0.5349$, and $\sigma_3 = 0.9047$. This configuration corresponds to the most likely trajectory for a series of random walks on the 5-dimensional potential energy surface [59].

Starting from this initial configuration, we vary the parameter σ_2 in order to reduce the size of the neck – and thus approach the limit of two orthonormal single-particle bases for each of the prefragments. In practice, the values of σ_2 were chosen such that the neck radius takes the values 0.04, 1.0, 1.25, 1.5, 1.75, 2.0 fm. Figure 9 gives a visual representation of these configurations. For the MC sampling, we use $n_{\mathrm{pair}} = 10000$ and $n_{\mathrm{loc}} = 1000$; together with our basis size of a $N_{\mathrm{sh}} = 30$ and a BCS threshold of $v_{\mathrm{thresh}}^2 = 10^{-5}$, this gives a statistical precision of approximately 0.5% on the charge and 0.15% on
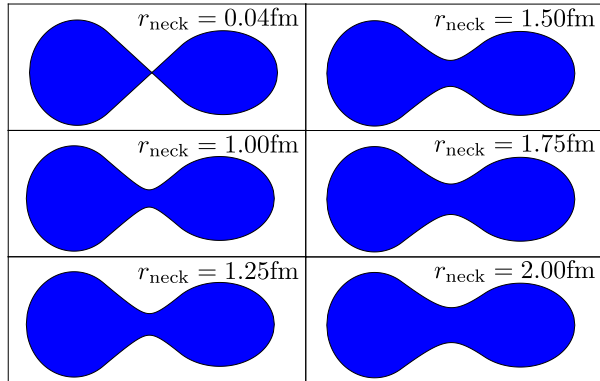
the mass fragmentation probabilities.

FIG. 9. Geometric shapes associated with the scission configurations of Table III.

TABLE III. Characteristics of scission configurations: neck radius, shape parameters and average mass/charge fragmentations of the left fragment.

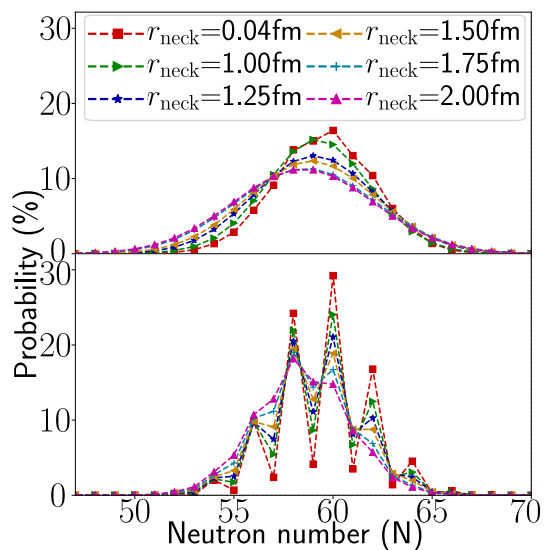| r_{neck}	α_2	α_3	σ_1	σ_2	σ_3	A_{L}	Z_{L}
0.04	0.448	0.6259	3.0613	-0.8431	0.9047	138.8	53.1
1.00	0.448	0.6259	3.0613	-0.7876	0.9047	139.5	53.5
1.25	0.448	0.6259	3.0613	-0.7576	0.9047	139.8	53.7
1.50	0.448	0.6259	3.0613	-0.7219	0.9047	140.1	53.8
1.75	0.448	0.6259	3.0613	-0.6812	0.9047	140.6	54.0
2.00	0.448	0.6259	3.0613	-0.6361	0.9047	141.4	54.3

FIG. 10. Upper panel: Neutron fragmentation probabilities (light fragment) for all the configurations listed in Table III obtained with our method. Lower panel: same probabilities obtained with the method presented in [24].

The neutron fragmentation probabilities are shown in Figure 10: the top panel shows results with MC sampling, while the bottom panel shows results with projec-
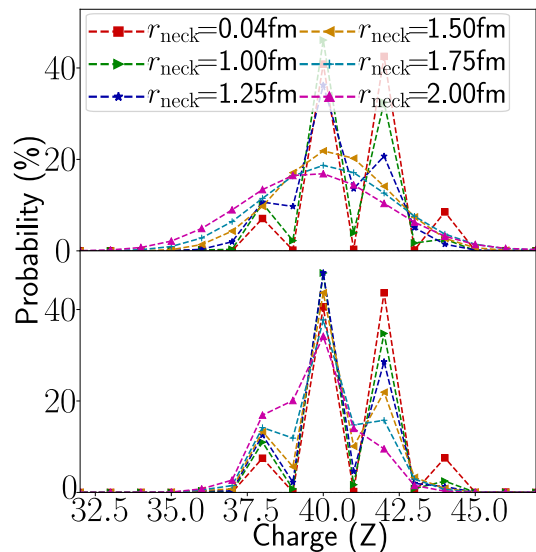

FIG. 11. Same as Figure 10 for the charge fragmentation probabilities (color online).

tors. We first note that there are substantial differences between the two approaches. Projectors yield an OES in the neutron fragmentations probabilities for $r_{\text{neck}} < 2.00$ fm. In contrast, there is no such OES in the sampling method except for very small values of the neck radius ($r_{\text{neck}} < 0.50$ fm).

The main explanation for this discrepancy is related to the parametrization of the nuclear surface. In generating the family of shapes of Figure 9, we started from the 3QS parameters corresponding to $r_{\text{neck}} = 2.5$ fm, and reduced *only* the value of σ_2 to obtain the other shapes. As a consequence of volume conservation, the fragments become more and more oblate with decreasing values of r_{neck}, which increases the value of the neutron Fermi energy. This facilitates tunneling for the states with energies around and above the Fermi level, even more so since pairing correlations for neutrons are rather high with our parametrization of the pairing force (the pairing gap is of the order of $\Delta_n \approx 2.25$ MeV for all configurations). This spurious "geometrical" effect could have been avoided with a more rigorous exploration of the nuclear shapes around our initial scission configuration, by making sure that, as we vary the size of the neck, all deformation parameters are adjusted so that the the energy remains a minimum. Such an exploration of the deformation space is automatic in self-consistent calculations, but should be done by hand in semi-phemenological methods. The cost of doing so in a a five-dimensional PES as the one we were working with is rather substantial.

Because of the Coulomb barrier, the proton Fermi energy is much lower than the top of the barrier between the two prefragments: tunneling is much less of an issue and protons are better localized. This could explain why the agreement between the two methods is much better for the charge fragmentation probabilities, as shown in Fig-

ure 11: the probability associated with an odd Z vanishes for a value of r_{neck} below 1.00 fm with both methods, and a strong odd-even staggering appears, at $r_{\text{neck}} = 1.25$ fm for the MC sampling and at $r_{\text{neck}} = 1.75$ with projectors. The quantitative agreement between the two approaches is in fact relatively good for $r_{\text{neck}} \leq 1$ fm.

B.   EDF Calculations

To gain further insight, we performed similar calculations in a fully microscopic framework. Specifically, we considered the scission configurations near the most likely fission of ^{240}Pu which are discussed extensively in Sec. IV of [15]. These configurations were obtained by performing constrained HFB calculations with $\langle \hat{Q}_{20} \rangle = 345$ b, and $\langle \hat{Q}_{\text{neck}} \rangle$ varying between 0.1 and 4.5. All calculations were performed with the Skyrme SkM* energy functional; numerical details such as the size and characteristics of the basis, the parameters of the pairing force, etc. can be found in [15].
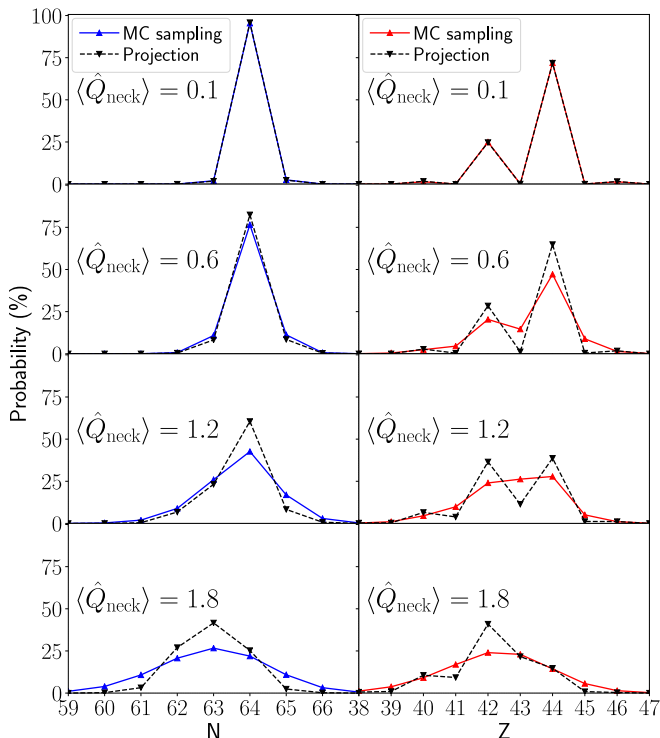

FIG. 12. Left panel: Comparison of the neutron fragmentation probabilities obtained with our Monte-Carlo sampling (full lines) and the projection method (dashed black lines) for different values of $\langle \hat{Q}_{\text{neck}} \rangle$. Right panel: same for the proton fragmentations (color online).

For each value of the Gaussian neck parameter, we used the double projection method to estimate the fragmentation probabilities of the system. We also computed the occupation probabilities v_k^2 in the canonical basis as well as the coefficients α_k of Eq.(8) needed for the MC method. Figure 12 summarizes the results for the proton and neutron fragmentation probabilities obtained in the two methods.

We note that the agreement between projection and MC sampling at the limit of very small necks is much better than in the macroscopic-microscopic approach. One might attribute this better agreement to the fact that in HFB calculations, the shapes of both the fissioning nucleus and the prefragments are automatically determined so that the energy of the fissioning system is minimum. As a consequence, such self-consistent calculations do not suffer from the geometrical artifact described in the previous section and the Fermi energy of both protons and neutrons does not vary much in the range of $\langle \hat{Q}_{\text{neck}} \rangle$ considered here, in contrast to the macroscopic-microscopic case.

V.   CONCLUSION

We have presented a new method to estimate the uncertainty of particle number in the fission fragments. It relies on sampling the probability distribution of finding N particles in the fragments based solely on the knowledge of a relevant single-particle basis for the fissioning nucleus together with occupation probabilities. We showed that our approach can be used to emulate results of particle number projection techniques, but also provides single-particle bases for each subsystem – provided the latter are sufficiently well separated. We emphasize that it is applicable both for Slater determinants and for generalized Slater determinants (= quasiparticle vacuum of the HFB theory), and is readily applicable when the energy states are not degenerate (e.g. when parity is internally broken). Indeed, when parity is conserved, single particles or quasiparticles are by definition spread over the two prefragments, and the splitting of the individual particle states might lead to non-orthogonal bases for each parition. In such cases, the degree of orthogonality of the basis within each partition should be tested to know if the Monte-Carlo sampling method is applicable.

We showed that restoring particle number in the prefragments formed at scission produces an odd-even staggering of probability fragmentations. When combined with full simulations of fission dynamics, this result could be key to reproducing the experimentally observed odd-even staggering of the charge distributions. In addition, restoring particle number could also be used to eliminate one of the free parameters typically associated with the calculations of fission fragment distributions (folding with a Gaussian, see [13]).

While we have illustrated our method in the case of the fission process of heavy atomic nuclei, it is in principle applicable to a much broader range of problems, such as, for example, the localization of electrons inside a molecule. In this case, space partitions would correspond to a small volume near each nucleus of the molecule, and we could calculate the number of electrons around each of them.

ACKNOWLEDGMENTS

[1] A. Bulgac, P. Magierski, K. J. Roche, and I. Stetcu, Phys. Rev. Lett. **116**, 122504 (2016).
[2] A. Bulgac, M. M. Forbes, S. Jin, R. N. Perez, and N. Schunck, Phys. Rev. C **97**, 044313 (2018).
[3] Y. Abe, S. Ayik, P. G. Reinhard, and E. Suraud, Phys. Rep. **275**, 49 (1996).
[4] P. Fröbrich and I. Gontchar, Phys. Rep. **292**, 131 (1998).
[5] M. D. Usang, F. A. Ivanyuk, C. Ishizuka, and S. Chiba, Phys. Rev. C **94**, 044602 (2016).
[6] J. Randrup, P. Möller, and A. J. Sierk, Phys. Rev. C **84**, 034613 (2011).
[7] J. Randrup and P. Möller, Phys. Rev. Lett. **106**, 132503 (2011).
[8] J. Randrup and P. Möller, Phys. Rev. C **88**, 064606 (2013).
[9] D. E. Ward, B. G. Carlsson, T. Døssing, P. Möller, J. Randrup, and S. Åberg, Phys. Rev. C **95**, 024618 (2017).
[10] J. F. Berger, M. Girod, and D. Gogny, Nucl. Phys. A **428**, 23 (1984).
[11] H. Goutte, J.-F. Berger, P. Casoli, and D. Gogny, Phys. Rev. C **71**, 024316 (2005).
[12] D. Regnier, M. Verrière, N. Dubray, and N. Schunck, Comput. Phys. Commun. **200**, 350 (2016).
[13] D. Regnier, N. Dubray, M. Verrière, and N. Schunck, Comput. Phys. Commun. **225**, 180 (2018).
[14] W. Younes and D. Gogny, Phys. Rev. Lett. **107**, 132501 (2011).
[15] N. Schunck, D. Duke, H. Carr, and A. Knoll, Phys. Rev. C **90**, 054305 (2014).
[16] N. Schunck and L. M. Robledo, Rep. Prog. Phys. **79**, 116301 (2016).
[17] A. S. Umar, V. E. Oberacker, J. A. Maruhn, and P.-G. Reinhard, J. Phys. G: Nucl. Part. Phys. **37**, 064037 (2010).
[18] C. Simenel and A. S. Umar, Phys. Rev. C **89**, 031601(R) (2014).
[19] P. Goddard, P. Stevenson, and A. Rios, Phys. Rev. C **92**, 054610 (2015).
[20] G. Scamps, C. Simenel, and D. Lacroix, Phys. Rev. C **92**, 011602(R) (2015).
[21] Y. Tanimura, D. Lacroix, and G. Scamps, Phys. Rev. C **92**, 034601 (2015).
[22] P. Goddard, P. Stevenson, and A. Rios, Phys. Rev. C **93**, 014620 (2016).
[23] Y. Tanimura, D. Lacroix, and S. Ayik, Phys. Rev. Lett. **118**, 152501 (2017).
[24] C. Simenel, Phys. Rev. Lett. **105**, 192701 (2010).
[25] G. Scamps and D. Lacroix, Phys. Rev. C **87**, 014605 (2013).
[26] K. Sekizawa and K. Yabana, Phys. Rev. C **88**, 014614 (2013).
[27] K. Sekizawa and K. Yabana, Phys. Rev. C **90**, 064614 (2014).
[28] P.N. Nadtochy and G.D. Adeev, Phys. Rev. C **72**, 054608 (2005).
[29] P. N. Nadtochy, A. Kelić, and K.-H. Schmidt, Phys. Rev. C **75**, 064614 (2007).
[30] J. Sadhukhan and S. Pal, Phys. Rev. C **84**, 044610 (2011).
[31] P. N. Nadtochy, E. G. Ryabov, A. E. Gegechkori, Y. A. Anischenko, and G. D. Adeev, Phys. Rev. C **85**, 064619 (2012).
[32] Y. Aritomo, S. Chiba, and K. Nishio, Prog. Nucl. Energy **85**, 568 (2015).
[33] J. Sadhukhan, W. Nazarewicz, and N. Schunck, Phys. Rev. C **93**, 011304(R) (2016).
[34] C. Ishizuka, M. D. Usang, F. A. Ivanyuk, J. A. Maruhn, K. Nishio, and S. Chiba, Phys. Rev. C **96**, 064616 (2017).
[35] A. J. Sierk, Phys. Rev. C **96**, 034603 (2017).
[36] M. D. Usang, F. A. Ivanyuk, C. Ishizuka, and S. Chiba, Phys. Rev. C **96**, 064617 (2017).
[37] P. Möller and T. Ichikawa, Eur. Phys. J. A **51**, 173 (2015).
[38] H. Goutte, P. Casoli, and J. F. Berger, Nucl. Phys. A **734**, 217 (2004).
[39] A. Zdeb, A. Dobrowolski, and M. Warda, Phys. Rev. C **95**, 054608 (2017).
[40] H. Tao, J. Zhao, Z. P. Li, T. Nikšić, and D. Vretenar, Phys. Rev. C **96**, 024319 (2017).
[41] J. Zhao, T. Nikšić, D. Vretenar, and S.-G. Zhou, Phys. Rev. C **99**, 014618 (2019).
[42] D. Regnier, N. Dubray, and N. Schunck, Phys. Rev. C **99**, 024611 (2019).
[43] H. Kleinert, *Path Integrals in Quantum Mechanics, Statistics, Polymer Physics, and Financial Markets* (World Scientific Publishing Co., 2009).
[44] P. Ring and P. Schuck, *The Nuclear Many-Body Problem*, Texts and Monographs in Physics (Springer, 2004).
[45] N. Schunck, *Energy density functional methods for atomic nuclei.*, IOP Expanding Physics (IOP Publishing, Bristol, UK, 2019) oCLC: 1034572493.
[46] J. Dobaczewski, M. V. Stoitsov, W. Nazarewicz, and P.-G. Reinhard, Phys. Rev. C **76**, 054315 (2007).
[47] L. M. Robledo, Phys. Rev. C **79**, 021302(R) (2009).
[48] R. N. Perez, N. Schunck, R. D. Lasseri, C. Zhang, and J. Sarich, Comput. Phys. Commun. **220**, 363 (2017).
[49] M. Anguiano, J. L. Egido, and L. M. Robledo, Nucl. Phys. A **696**, 467 (2001).
[50] J.A. Sheikh, P. Ring, E. Lopes, and R. Rossignoli, Phys.

Rev. C **66**, 044318 (2002).

[51] M. Stoitsov, J. Dobaczewski, W. Nazarewicz, and P. Ring, Comput. Phys. Commun. **167**, 43 (2005).

[52] J. R. Nix, Nucl. Phys. A **130**, 241 (1969).

[53] J. R. Nix, Annu. Rev. Nucl. Sci. **22**, 65 (1972).

[54] R. Hasse and W. Myers, *Geometrical relationships of macroscopic nuclear physics*, 1st ed., Springer Series in Nuclear and Particle Physics (Springer-Verlag Berlin Heidelberg, 1988).

[55] P. Möller, A. J. Sierk, T. Ichikawa, and H. Sagawa,

Atom. Data Nuc. Data Tab. **109**, 1 (2016).

[56] J. F. Berger, J. D. Anderson, P. Bonche, and M. S. Weiss, Phys. Rev. C **41**, R2483 (1990).

[57] P. Schillebeeckx, C. Wagemans, A. J. Deruytter, and R. Barthélémy, Nucl. Phys. A **545**, 623 (1992).

[58] K. Nishio, Y. Nakagome, I. Kanno, and I. Kimura, J. Nuc. Sci. Tech. **32**, 404 (1995).

[59] M. Verrière, M. Mumpower, and T. Kawano, "Analysis of fission fragment yield models for the actinides," In preparation (2019).